Mechanosynthesis of metastable cubic δ-$Ta_{1-x}N$

T. Garcia-Mendoza [a], A. Martinez-Garcia [b,c],

I. G. Becerril-Juarez [d], E. Lopez-Vazquez [c], M. Avalos-Borja [d],

M. Valera-Zaragoza [b], E. A. Juarez-Arellano [b,e]

[a] *División de Estudios de Posgrado, Maestría en Ciencias Químicas, Universidad del Papaloapan, Circuito Central 200, Parque Industrial, 68301, Tuxtepec, Oaxaca, México.*

[b] *Instituto de Química Aplicada, Universidad del Papaloapan, Circuito Central 200, Parque Industrial, 68301, Tuxtepec, Oaxaca, México.*

[c] *Tecnológico Nacional de México, Instituto Tecnológico de Oaxaca, Av. Víctor Bravo Ahuja 125, 68030, Oaxaca, México.*

[d] *División de Materiales Avanzados, Instituto Potosino de Investigación Científica y Tecnológica, San Luis Potosí, México.*

[e] *Corresponding author: E. A. Juarez-Arellano, eajuarez@unpa.edu.mx*

Abstract

The formation of the cubic δ-$Ta_{1-x}N$ phase by high-energy ball-milling from tantalum and boron nitride (h-BN) is explored. Two different molar ratios Ta:BN, 1:1 and 2:1, were used. X-ray diffraction, scanning electron microscopy, surface area analysis by the Brunauer-Emmett-Teller method, and thermogravimetric analysis were used to characterize the products obtained. In both molar ratios and after a few minutes of milling, the mechanosynthesis of δ-$Ta_{1-x}N$ was observed. Increasing the entropy of the system by introducing vacancies and point defects by the high-energy ball-milling process seems to stabilize the cubic δ-$Ta_{1-x}N$ phase, as previous

theoretical studies had reported. The phase obtained depends on the molar ratio used: in the molar ratio 1:1 a non-stoichiometric δ-$Ta_{1-x}N$ phase is obtained, while in the molar ratio 2:1 a stoichiometric δ-TaN phase and secondary phases are obtained. The amorphous boron remains dispersed in the material until the mechanical energy is high enough to trigger the formation of tantalum borides.

Key words:

cubic δ-$Ta_{1-x}N$ phase, high-energy ball-milling, metastable phase, tantalum nitride

---

1 Introduction

In recent years, materials with the combination of light elements and transition metals have gained interest, especially carbides, borides, and nitrides (Friedrich et al. 2011). These materials show high hardness, high melting points, high thermal and chemical stability, high resistance to corrosion, good electrical conductivity and interesting magnetic properties (Pierson 1996, Oyama 1996, Tian et al. 2012, Escobar et al. 2014, Fahrenholtz and Hilmas 2017). Among the binary transition metal nitrides, tantalum nitrides are some of the most widely used nitrides. Tantalum nitrides have been used as visible light photocatalysts (Wang et al. 2012), diffusion barriers (Takeyama 1996, Laurila et al. 2002), electrical resistances (Lu et al. 2001), resistors (Lee et al. 2018), electrodes in CMOS (Complementary Metal Oxide Semi-conductor) (Lemberger et al. 2007), tool protective coatings (Gladczuk et al. 2004), π-type attenuators (Cuong et al. 2006), biomedical applications (Leng et al. 2001, Jin et al. 2018), within other applications.

The tantalum-nitrogen system is very complex, it contains numerous phases and, to this day, there is only an early stage phase diagram (Gatterer et al.

1975, Frisk 1998). Ta-N exhibits different phases such as ε-TaN ($P\bar{6}2m$, CoSn-type crystal structure), δ-TaN ($Fm\bar{3}m$, NaCl-type), ϑ-TaN ($P\bar{6}m2$, WC-type), β-Ta_2N ($P\bar{3}1m$, CdI_2-type), Ta_5N_6 ($P6_3/mmc$), Ta_3N_5 (Cmcm), and Ta_4N_5 (I4/m) (Friedrich et al. 2010; 2013). The Ta-N system also has some high pressure phases such as η-Ta_2N_3 (Pbnm), Ta_3N_5 (Pnma, U_3Se_5-type), and Ta_3N_5 (Pnma, U_3Te_5-type) (Friedrich et al. 2010, Salamat et al. 2014).

Several methods have been used to synthesize tantalum nitrides, although the obtained Ta-N compound or the mixture of them depends on the method used. For example: magnetron sputtering deposition stabilize β-Ta_2N, ε-TaN, and Ta_3N_5 phases (Leng et al. 2001, Cuong et al. 2006), self-propagating high temperature synthesis - SHS (ε-TaN, β-Ta_2N) (Yeh et al. 2004), rapid thermal processing (β-Ta_2N, ε-TaN, Ta_3N_5) (Angelkort et al. 2003), arc discharge (β-Ta_2N, δ-TaN) (Shen and Wang 2011), combustion (ε-TaN, β-Ta_2N, ϑ-TaN, δ-TaN) (Lee et al. 2013), homogeneous reduction in liquid ammonia (ε-TaN, β-Ta_2N, δ-TaN) (Liu et al. 2012), Reactions under Autogenic Pressure at Elevated Temperature - RAPET (δ-TaN) (George et al. 2009), laser heating diamond anvil cell - LHDAC (β-Ta_2N, η-Ta_2N_3, ϑ-TaN) (Friedrich et al. 2010; 2013), or mechanosynthesis (β-Ta_2N, Ta_3N_5) (Qin et al. 1998), among other synthesis methods.

According to Liu et al. (2012), the cubic δ-TaN phase is the Ta-N compound with the best physical properties such as stability at high temperature, superconductivity, and high hardness. δ-TaN exhibits one of the highest hardness of the group of transition metal mononitrides, 26 GPa (Yang et al. 2016). However, the phase is often obtained in mixtures with other Ta-N compounds, so it is difficult to synthesize it as a single phase. The cubic δ-TaN is considered a high-temperature metastable phase. It can be formed from ε-TaN as

starting material either at 2273K and 0.001 GPa nitrogen pressure (Gatterer et al. 1975), at 2073K and 3-10 GPa (Boiko and Popova 1970), or by shock compression (Mashimo et al. 1993). δ-TaN can be also formed from different starting material or mixtures such as a mixture of $TaCl_5$-Li_3N-NaN_3 during rapid solid-state metathesis (Gillan and Kaner 1994), from the reduction of $TaCl_5$ in liquid NH_3 at 1445 K (Ma et al. 2007), from the combustion of K_2TaF_7-NaN_3-NH_4F at 2 MPa nitrogen pressure (Lee et al. 2013), from tantalum irradiated with highly energetic nitrogen ions (Ensinger et al. 1995), from tantalum and pure nitrogen gas in DC arc-discharge (Shen and Wang 2011), or from tantalum at 0.2-1.82 MPa nitrogen pressure and 425-575 K by SHS (Yeh et al. 2004).

It has been reported that one way to stabilize the cubic δ-TaN phase is increasing the entropy of the system by introducing vacancies and point defects (Koutná et al. 2016). Koutná et al. (2016) demonstrated, by ab initio calculations, a strong tendency to form metal vacancies in the cubic B1 δ-TaN structure. The most stable composition $Ta_{0.78}N$ contains $\sim$11% of metal vacancies. Pacher et al. (2017) showed, by first-principles calculations, that increasing the number of vacancies changes the stability phase field of Ta-N from ε-TaN, to ϑ-TaN, and finally to δ-TaN. They also report that the phase field of the rock-salt cubic metastable Ta-Al-N and Nb-Al-N phases increases with the number of vacancies. Similar results have been predicted in the Ta-C-N system by DFT calculations and corroborated experimentally by magnetron sputtered Ta-C-N thin films (Glechner et al. 2018).

High-energy ball-milling is known to access metastable phases and to introduce structural defects during the process (Granados-Fitch et al. 2016, Kakazey et al. 2016, Martinez-Garcia et al. 2019). Thus high-energy ball-milling seems

to be an excellent method to synthesize and stabilize the cubic δ-TaN phase. However, there is only one report of the reaction of tantalum and nitrogen gas in a high-energy ball-milling, but those experiments lead to the formation of a mixture of β-Ta_2N and Ta_3N_5 phases (Qin et al. 1998). Besides, the strong $N \equiv N$ triple bond results in the difficulty of converting N_2 into other compounds. Thus, in this study, we explore the formation of the cubic δ-TaN phase by high-energy ball-milling from tantalum and boron nitride (h-BN). Two different stoichiometric ratios Ta:BN were used 1:1 and 2:1. In both cases, the mechanosynthesis of δ-TaN was observed after a few minutes of milling. The products obtained were characterized by X-ray diffraction (XRD), scanning electron microscopy (SEM), surface area analysis by the Brunauer-Emmett-Teller (BET) method, and thermogravimetric analysis (TGA).

2 Experimental

Tantalum (Sigma-Aldrich, 99.9%) and hexagonal boron nitride (h-BN, Sigma-Aldrich, 98%) powders in the molar ratio of 1:1 and 2:1 were homogenized in an agate mortar and were put in the milling vials. The same procedure was followed by the systems Ta-B (1:1 and 1:2), Ta-C (1:1 and 2:1), and Ta-B-C (1:1:1 and 1:2:1). Boron (Sigma-Aldrich, 99%) and carbon (graphite, Sigma-Aldrich, 99.9%) were used.

The high-energy ball-milling treatment was carried out in air (in hermetically sealed vials) in a planetary ball-mill (Pulverisette 7 premium line, Fritsch). Vials (80 ml) and balls (15 of 1 cm) of tungsten carbide grinding materials were used. A rotation rate of 600 rpm and different milling times were used. A ball to powder ratio of 115:1 was used. In order to avoid overheating, the

milling was done in cycles of 5 min milling and 15 min pause for cooling.

2.1 Characterization

The evolution of the reaction has been followed by X-ray diffraction. X-ray powder diffraction (XRD) patterns were collected in air and at ambient temperature in a Bruker D-8 Advance diffractometer with Cu$K_{\alpha 1}K_{\alpha 2}$ radiation. Sodium iodide (NaI) scintillation detector and flat polymer sample holder were used. The 2θ-interval explored was 10° - 90° with 0.1° step size, 5s counting time, continuous mode, and spinning of 15 rpm. The Le Bail fits and Rietveld refinement were performed using the program FULLPROF (Rodriguez-Carvajal 1993). Linear interpolation between approximately 30 manually selected points for the background and a pseudo-Voigt profile function were used.

Fourier-transformed infrared (FT-IR) spectra were collected in a Spectrum 100 Perkin Elmer spectrometer with an ATR accessory, using a resolution of 4 cm^{-1} in a range of 4000-550 cm^{-1}.

The morphology and characteristics of the surface of the samples were observed by Scanning Electron Microscopy using a Dual Beam (FIB/SEM) FEI Helios Nanolab 600 equipped with an energy-dispersive X-ray spectroscopy (EDS) detector. Uncoated samples were mounted on aluminum stubs with double-sided sticking carbon tape. Several regions of the sample were selected for the measurements.

The specific surface area was obtained by the BET method (N_2 adsorption at 63 K) using a porosity measuring system BELSORP-mini equipment surface area equipment. The samples were degassed at 573 K in an inert atmosphere

(N_2).

Thermogravimetric Analysis (TGA) was carried out using a Perkin Elmer STA 6000 simultaneous thermal analyzer. 10-20 mg of sample was placed in an open alumina pan and analyzed with N_2 atmosphere (20 mL/min) in the temperature interval between 373 K to 1073 K at 10 K/min.

3 Results and Discussion

The powder diffraction patterns from tantalum, boron nitride (h-BN), and the mixtures in the molar ratio of 1:1 and 2:1 during high-energy ball-milling up to 30 min can be seen in Figures 1(a-b), while the lattice parameters are shown in Table 1. The diffractograms show that the formation of δ-TaN can be detected after 10 min of milling, while the full reaction is observed after 20 min of milling, indistinctly of the molar ratio used. The lattice parameters obtained for δ-TaN agrees to what has been reported in the literature, Table 1. The main difference in the diffraction patterns of the samples with molar ratio 1:1 and 2:1 is that in 2:1 is observed the presence of WC from the milling material. The mechanosynthesis process was repeated several times to evaluate the reproducibility of the method (Figures 1c-d). In every repetition, the presence of WC was only observed in the samples with a molar ratio of 2:1. Yang et al. (2016) reported, based on magnetron sputtering experiments, that the hardness of δ-TaN layers decreases with the increment of metal vacancies. They report a hardness of 26 GPa for δ-TaN, 18.2 GPa for δ-$Ta_{0.82}N$ and 14.7 GPa for δ-$Ta_{0.67}N$. Also, the hardness of the mechanosynthesized δ-TaN could be higher than the values reported by Yang et al. (2016) due to the Hall-Petch effect (Oganov et al. 2014), where the hardness increases as the

particle size decrease. Thus, in the experiments with a molar ratio 2:1 is very likely to have the formation of stoichiometric δ-TaN with a hardness similar or greater than the milling material (WC - 22-28 GPa, (Friedrich et al. 2011)) generating contamination from the milling material in the final product; while in the experiments with molar ratio 1:1 is very likely to have the formation of non-stoichiometric δ-$Ta_{1-x}N$ with metal vacancies.

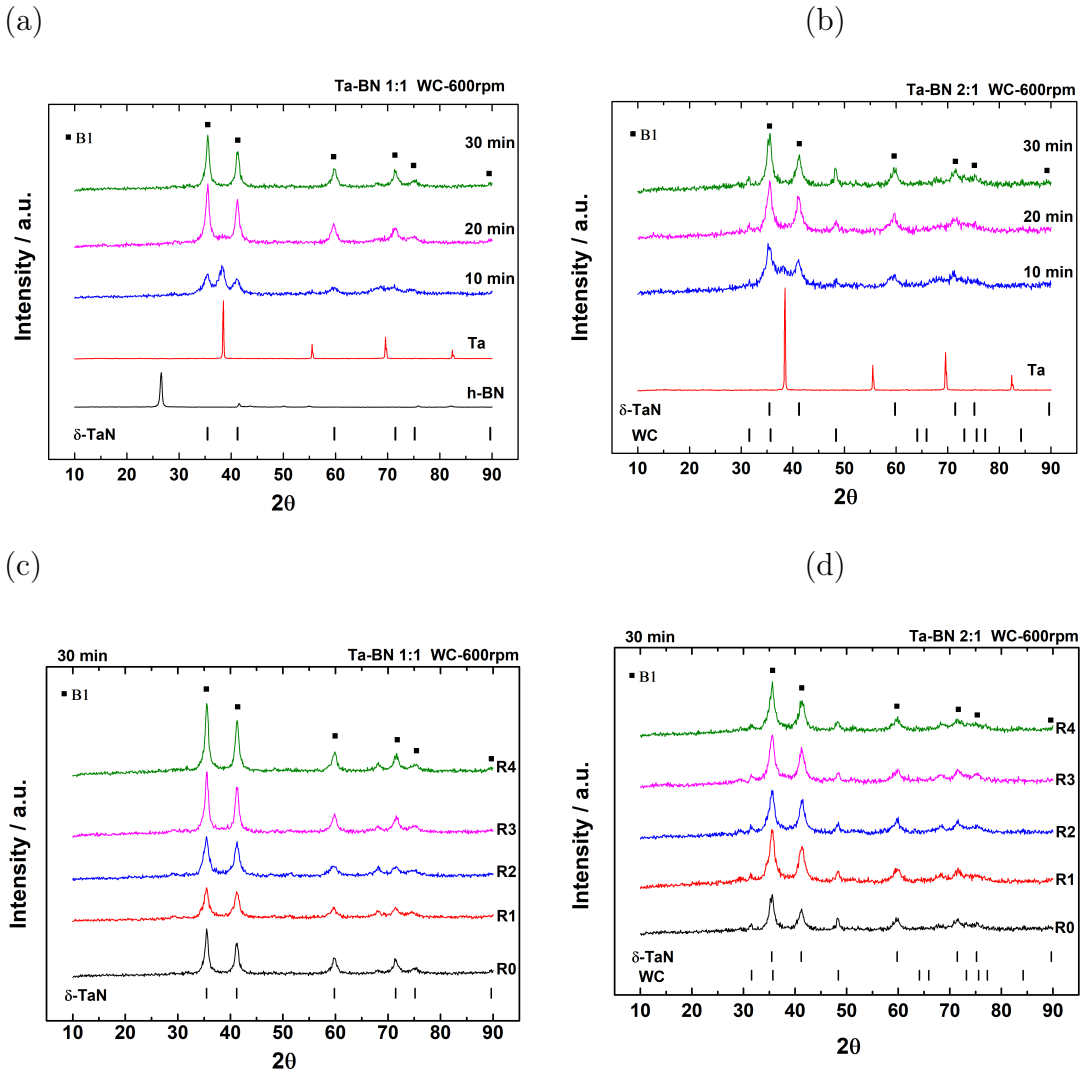

Fig. 1. X-ray powder diffraction patterns of Ta-BN ((a) 1:1 and (b) 2:1) before and after high-energy ball-milling, see Table 1. The Ta-BN ((c) 1:1 and (d) 2:1) mechanosynthesis was performed several times in order to evaluate the reproducibility.

If the milling is extended, the formation of orthorhombic TaB (o-TaB) is observed at 40 min of milling in the mixture with a molar ratio 1:1. The Rietveld refinement of this sample is shown in Figure 2, while the lattice parameters and crystal structure are shown in Table 2. The values of the lattice parameters obtained here agrees with what is reported. For example, the lattice parameters of o-TaB (a = 3.28 Å, b = 8.67 Å, c = 3.15 Å, ICSD-602892) and WC (a = 2.90 Å, c = 2.85 Å, ICSD-246149) are in a good agreement with the values shown in Table 2. Furthermore, the refinement of the site occupancy of tantalum in δ-TaN gives an approximate composition of δ-$Ta_{0.84(1)}N$, which support the idea of the formation of non-stoichiometric δ-$Ta_{1-x}N$ when a molar ratio 1:1 is used.

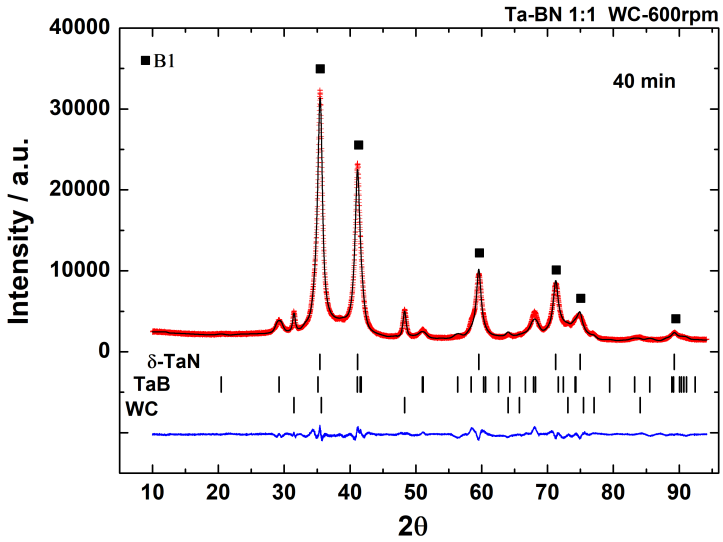

Fig. 2. Rietveld refinement of the X-ray powder diffraction patterns of Ta-BN (1:1) after 40 min of high-energy ball-milling, see Table 2. The formation of orthorhombic TaB (o-TaB) is observed at 40 min of milling.

The question that arises is whether δ-TaN is actually formed or whether a tantalum boron nitride or a cubic tantalum boride is obtained instead during the mechanosynthesis. Infrared spectra of Ta, h-BN, and Ta-BN (1:1, at different

milling times) are shown in Figure 3. The characteristic bands of *h*-BN appear at 1374 cm^{-1} (E_{1u} in-plane B-N stretching vibration) and 778 cm^{-1} (A_{1u} B-N-B out-of-plane bending vibration) (Zhai et al. 2019). These vibrational modes have been attributed to the sp^2 bonded *h*-BN (Aradi et al. 2014). However, these bands vanished when the Ta-BN (1:1) mixture is ball-milled. At 30 min of milling, the characteristic bands of *h*-BN disappear, which indicates that at these conditions, there are no B-N or B-N-B links left. According to X-ray diffraction (Figure 1a), the reaction of tantalum is also complete at 30 min of milling. These results indicate that the breakdown of *h*-BN and the formation of δ-TaN are correlated.

The enthalpies of formation reported for δ-TaN, o-TaB, and h-TaB_2 are -119 – -128 $kJmol^{-1}$, -78 – -83 $kJmol^{-1}$, and -55 – -74 $kJmol^{-1}$, respectively (Niessen and Boer 1981, Meschel and Kleppa 2001, Li et al. 2014, OuYang et al. 2017). Therefore, by those enthalpies, the δ-TaN structure is energetically more stable than o-TaB or h-TaB_2 structures. Therefore, the δ-TaN structure is formed first during the mechanosynthesis process.

Regarding the formation of a cubic tantalum boride during the mechanosynthesis. It has been reported that the Ta-B system contains several phases (Ta_2B, Ta_3B_2, Ta_5B_6, Ta_3B_4 (Winkler et al. 2010)), although none of them is cubic. Besides, there are no reports of the formation of any ternary TaBN compound. Nevertheless, there are few reports of tantalum boron nitride films where TaB_2 and N_2/Ar were deposited on silicon substrates by radio frequency reactive sputtering; however, the final composition of the films is a mixture of TaB_2, TaN and BN phases (Lin and Lee 2003, Goncharov et al. 2008).

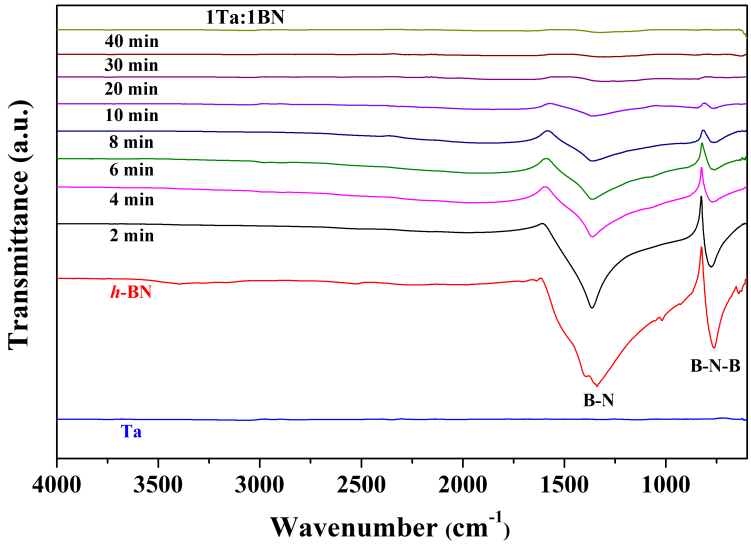

Fig. 3. Infrared spectra of Ta, *h*-BN, and Ta-BN (1:1, at different milling times). The characteristic absorption bands of *h*-BN are indicated.

Savyak et al. (2018) reported the reaction of elemental tantalum and boron by high-energy ball-milling. They reported the formation of crystalline o-TaB after 10 min of milling in samples with a molar ratio of 1:1, and poorly crystalline hexagonal TaB_2 (h-TaB_2) after 50 min in samples with a molar ratio 1:2. However, different ball-mill equipment was used, and therefore the energy supplied by the ball-mill used by Savyak et al. (2018) differs from the used in this study. Thus, in order to corroborate this behavior, and to clarify the role of boron from the h-BN starting material, the reaction of tantalum and boron mixtures in the molar ratios of 1:1 and 1:2 were evaluated up to 30 min of milling, Figure 4. The lattice parameters of the products are shown in Table 3. The formation of poorly crystalline o-TaB is observed after 20 min of milling in the sample with a molar ratio of 1:1, Figure 4a; while, the formation poorly crystalline o-TaB and h-TaB_2 are observed at 10 min in the molar ratio 1:2, Figure 4b.

The results of the mechanosynthesis of tantalum and boron corroborate that it leads to the formation of o-TaB or o-TaB/h-TaB_2, depending on the mo-

lar ratio used; and that none of the others Ta-B intermediate phases or the formation of a new B1-TaB phase are observed. However, the milling times at which the o-TaB phase is obtained in the molar ratio of 1:1 changes from 10 min using Ta+B (Savyak et al. 2018), to 20 min using Ta+B (this study) or to 40 min using Ta+c-BN (this study). The use of different milling conditions and ball-mill equipment could explain the variation between the results of Ta+B of Savyak et al. (2018) and this study. However, the same milling conditions were used in Ta+B (20 min) and Ta+c-BN (40 min). Therefore, the variation between these results could be associated with different diffusion kinetics (c-BN vs. B).

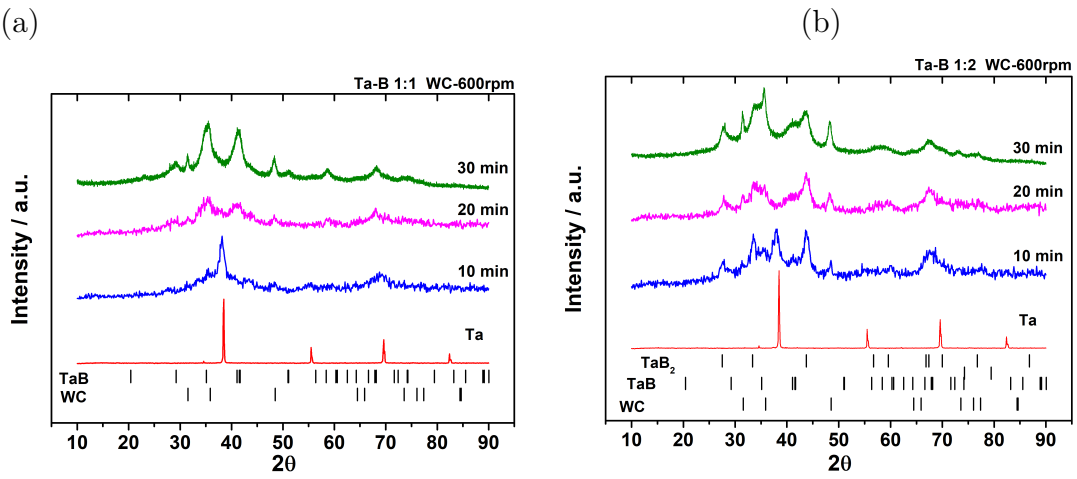

Fig. 4. X-ray powder diffraction patterns of Ta-B ((a) 1:1 and (b) 1:2) before and after high-energy ball-milling up to 30 min, see Table 3. The formation of orthorhombic TaB (o-TaB) and hexagonal TaB_2 (h-TaB_2) phases is observed.

The experiment that would confirm the formation of δ-TaN over o-TaB, and h-TaB_2 could be the mechanosynthesis of a mechanical mixture of Ta-B-N. However, using N_2 gas as a precursor is not an option due to the strong $N \equiv N$ triple bond that has to be broken. Also, using another nitrogen source such as ammonium or hydrazinium could lead to different chemical equilibrium. However,

an indirect way to do this experiment is by replacing nitrogen with carbon. It has been reported that the Ta-C system contains two intermediate stoichiometric phases (TaC: B1-type structure, and Ta_2C: trigonal CdI_2-type), and one non-stoichiometric phase (ζ-Ta_4C_3) (Bayarjargal et al. 2014, Gusev et al. 2007); while there are no reports of the formation of any ternary TaBC compound. Thus, mechanical mixtures of Ta-C (1:1), Ta-C (2:1), Ta-B-C (1:1:1), and Ta-B-C (1:2:1) were prepared from the elements and ball-milled up to 30 min, using the same milling conditions than before. The powder diffraction patterns are shown in Figures 5 and 6, while the lattice parameters of the products are shown in Table 3.

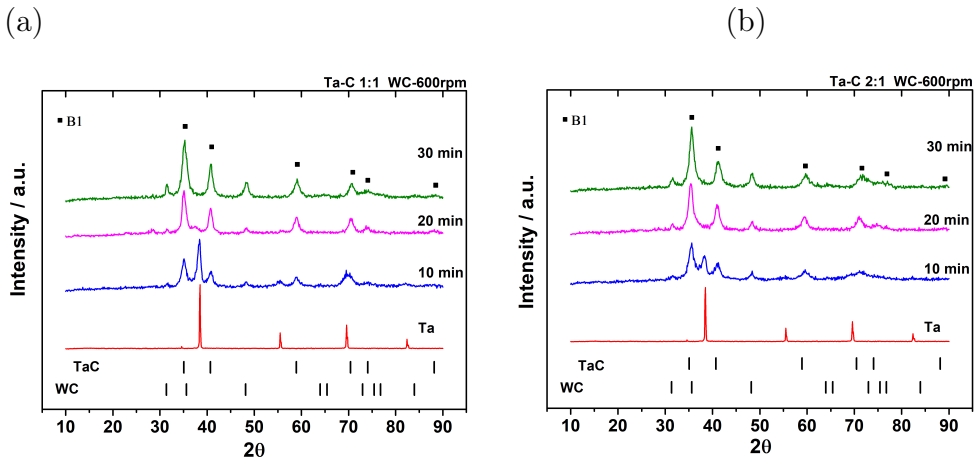

Fig. 5. Le Bail fits of the X-ray powder diffraction patterns of Ta-C ((a) 1:1 and (b) 1:2) before and after high-energy ball-milling up to 30 min, see Table 3.

In the Ta-C (1:1) and Ta-C (2:1) systems, the partial formation of the TaC (B1-type structure) is observed after 10 min of milling, while the full reaction is observed after 30 min of milling, Figure 5. No other tantalum carbide phase is observed. The variation in the Ta:C ratio also does not affect the phase formation. In the Ta-B-C (1:1:1) system, the formation of TaC (B1-type structure) is observed at 10 min of milling, while the full reaction at 20 min of milling.

Besides contamination from the milling material (WC), no other phases are observed. However, in the Ta-B-C (1:2:1) system, the formation of h-TaB_2 is detected from the 10 min of milling, Figure 6. To corroborate these results, the mechanosynthesis of Ta-B-C-1:1:1 and Ta-B-C-1:2:1 were repeated four times, Figure 6 and Table 4. Through all the repetitions, the results were always consistent. Therefore, when the molar ratios are 2Ta:1BN, 1Ta:1BN or 1Ta:1B:1C the phases obtained during the mechanosynthesis are δ-TaN and B1-TaC (Figures 1 and 6). The boron must be amorphous and dispersed in the material, and when the mechanical energy is high enough, then it reacts (Figure 2). However, when the content of boron is higher than the rest (1Ta:2B:1C), then a mixture of phases (B1-TaC and h-TaB_2) is obtained simultaneously (Figure 6).

3.1 Characterization of Ta-BN products (1:1 and 2:1)

A general view, representative of the Ta-BN mixtures after 30 min of ball-milling, is shown in the micrographs of Figure 7. The samples consist of agglomerates of different sizes (Figure 7(a-b)). At higher magnification, it is observed that the agglomerates are predominantly composed of spherical particles of different sizes (Figure 7(c-d)). In the sample with a molar ratio of 1:1, the spherical particles are more defined and less sintered than the 2:1 sample. Liu et al. (2012) and George et al. (2009) also reported a spherical morphology in the δ-TaN phase obtained by them.

EDS analyzes were performed to determine the chemical composition of the agglomerates (Figure 7(e-f)). In the EDS spectra, the elements present were

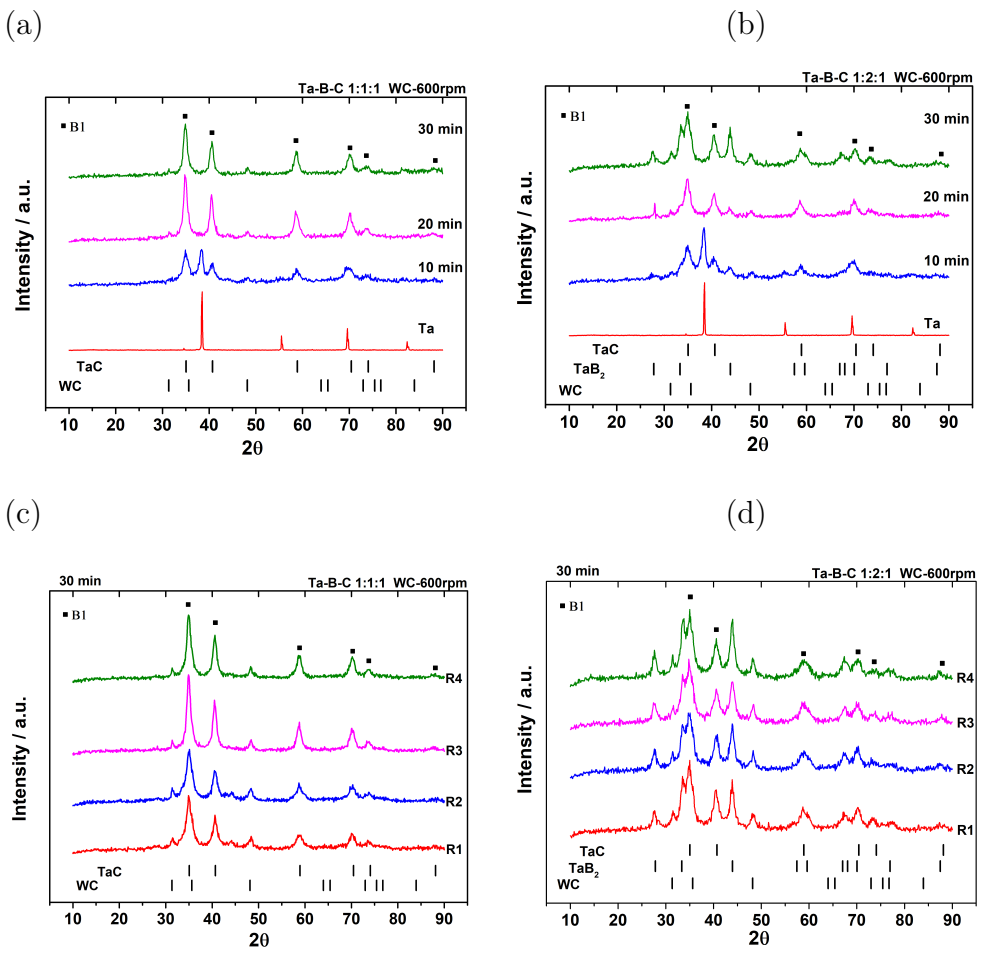

Fig. 6. Le Bail fits of the X-ray powder diffraction patterns of Ta-B-C ((a) 1:1:1 and (b) 1:2:1) before and after high-energy ball-milling up to 30 min, see Table 3. The repetition of Ta-B-C ((c) 1:1:1 and (d) 1:2:1) mechanosynthesis was performed several times in order to evaluate the reproducibility of the mechanosynthesis, see Table 4.

Ta, N, B, and O. The sensitivity of EDS analysis is higher for heavy atoms than for light atoms, whose concentrations are generally underestimated. Thus, the intention of this EDS analysis is more qualitatively, and it shows that no contamination is present in the samples.

The nitrogen adsorption/desorption isotherms of Ta-BN 1:1 and 2:1 are shown in Figure 8. BET analysis showed that the samples Ta-BN 1:1 and 2:1 have a BET surface area of 1.85 m^2/g and 0.16 m^2/g, respectively. These results are consistent with the micrographs (Figure 7), where the spherical particles in

the Ta-BN 1:1 sample are more defined and less sintered than the 2:1 sample; therefore with mayor surface area. However, even though both samples have particles of the order of nanometers, the surface area is low, possibly because the agglomerates do not have cracks, large pores, or free interfaces.

The nitrogen adsorption/desorption isotherms of both samples show a type III isotherm according to the International Union of Pure and Applied Chemistry (IUPAC) classification (Thommes et al. 2015). This type of isotherm is characteristic of nonporous or macroporous materials and indicates an unrestricted multilayer formation process (Gregg and Sing 1982). This behavior indicates that the adsorption is associated with capillary condensation and is not limited to high relative pressures (p/p_0). In such a case, adsorbate-adsorbent interactions play an essential role during the adsorption process due to weak gas-solid interaction; the adsorbed molecules clustered around the most favorable sites on the surface of nonporous or macroporous solids (Thommes et al. 2015, Gregg and Sing 1982).

The Ta-BN 1:1 isotherms show a significant hysteresis type H3 (Figure 8(a)). Sing and Williams (2004) reported that in the case of N_2 adsorption at 77 K, H3 loops have characteristic desorption shoulders and lower closure points in the region of $0.42P_0$, which is associated with blocked mesopores. In the Ta-BN 1:1 sample, this shoulder is observed at $\sim 0.45P_0$ (Figure 8(a)). Groen et al. (2003) reported that the step-wise desorption isotherm is because the encapsulated mesopores empty at a lower pressure than the open pores of similar size. Thus, the isotherm of Ta-BN 1:1 suggests that the sample con-

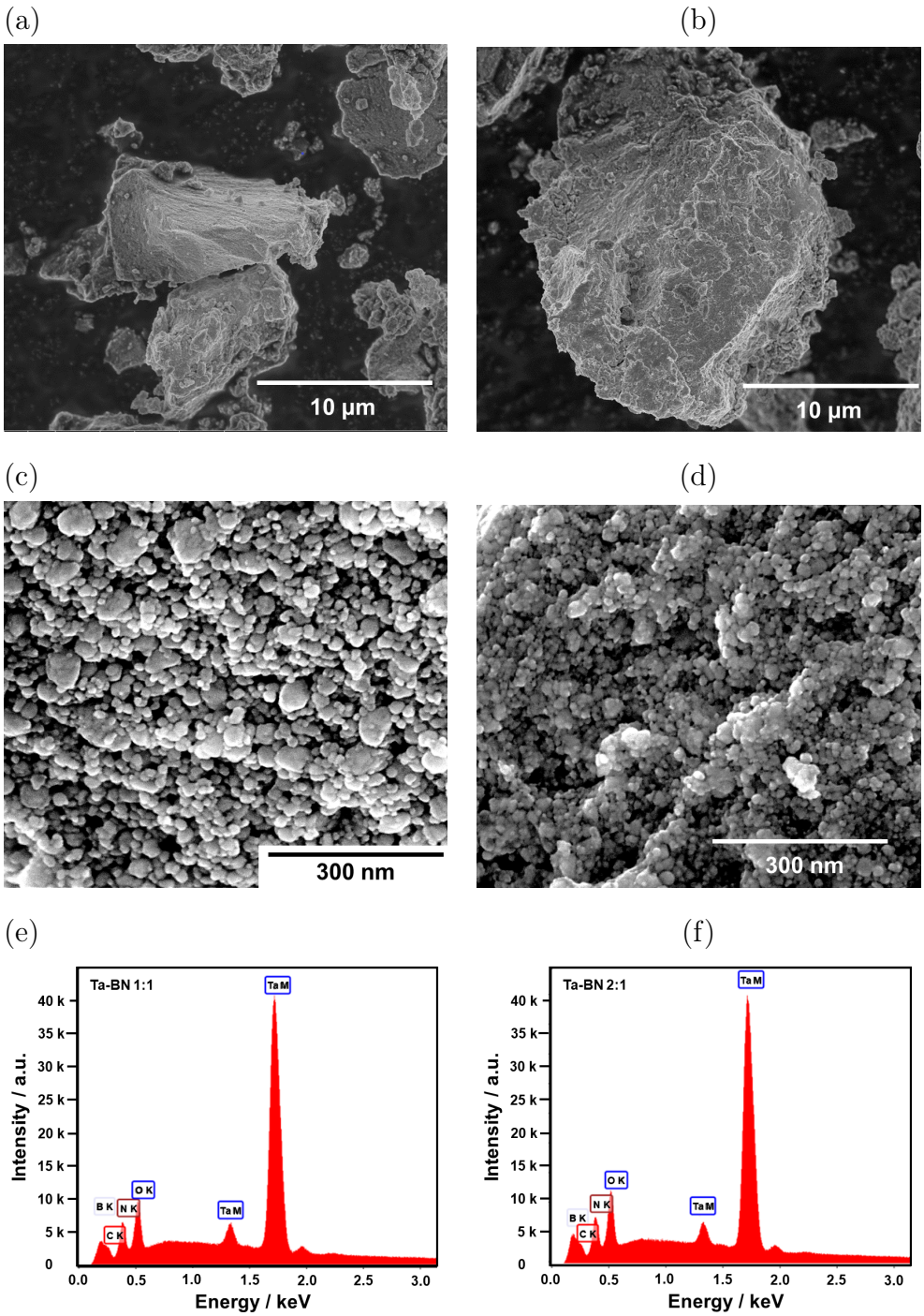

Fig. 7. SEM micrographs and EDS of the products of the mechanosynthesis after 30 min of Ta-BN mixtures (a,c,d) 1:1 and (b,d,e) 2:1.

tains blocked mesopores, which could also be associated with the less sintered appearance observed in the scanning electron micrographs (Figure 7(c)).

The thermal behavior of Ta-BN 1:1 and Ta-BN 2:1 after 30 min of milling

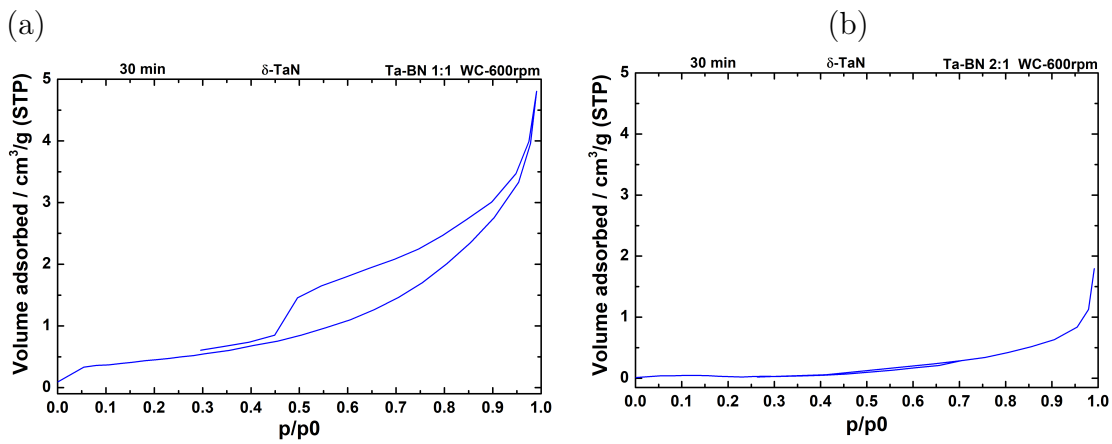

Fig. 8. Nitrogen adsorption and desorption isotherms for the calculation of the specific surface area by the BET method of the products of the mechanosynthesis after 30 min of Ta-BN mixtures (a) 1:1 and (b) 2:1.

is shown in Figure 9. The weight loss curve (TGA) of Ta-BN 1:1 shows two stages. The first stage is a weight loss of 0.6% associated with the dehydration of the sample. The second stage is a 1.3% weight gain starting at around 850 K (Figure 9(a)). On the other hand, the weight loss curve (TGA) of Ta-BN 2:1 shows only one stage. The stage is a 1.2% weight gain starting at around 900 K (Figure 9(b)). In both stoichiometric relationships, the mass increment and the temperature at which it occurs are around the same; therefore, we consider that the mass increment is due to the interaction of boron with the N_2 gas (buoyancy and drag) used in TGA measurements. Mirkarimi et al. (1997) reported that the optimal temperature to form c-BN thin films by CVD process is between 700 K and 800 K. This temperature region is also in agreement with the B-N phase diagram reported by Mujica et al. (2003).

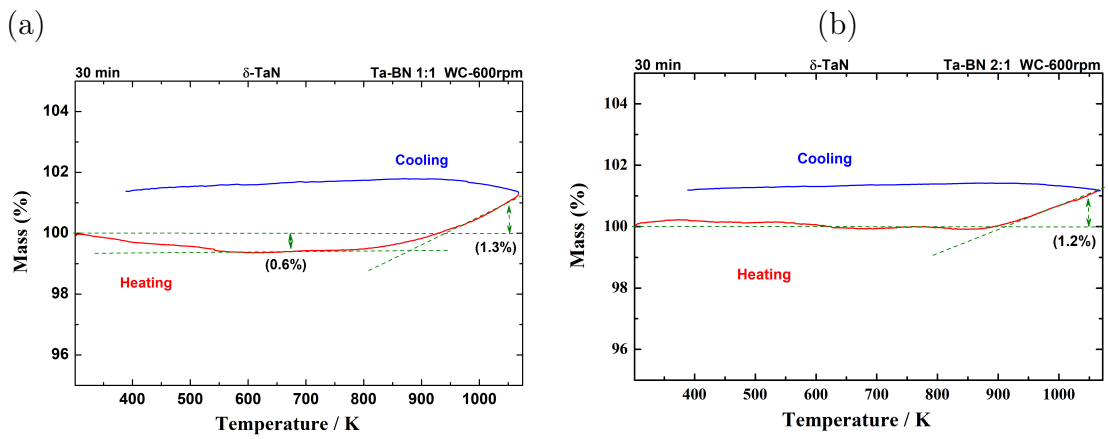

Fig. 9. TGA weight loss curves of the products of the mechanosynthesis after 30 min of Ta-BN mixtures (a) 1:1 and (b) 2:1.

4 Conclusions

The mechanosynthesis of δ-$Ta_{1-x}N$ was successfully completed from mixtures of tantalum and boron nitride (h-BN). The defects induced during the high-energy ball-milling process seems to stabilize the cubic δ-$Ta_{1-x}N$ phase, which agrees with previous theoretical studies that suggest that increasing the entropy of the system by introducing vacancies and point defects would stabilize the δ-TaN phase. A molar ratio of 1Ta:1BN leads to the formation of a non-stoichiometric δ-$Ta_{1-x}N$ phase, while a molar ratio of 2Ta:1BN leads, most probable, to a stoichiometric δ-TaN phase. After the formation of δ-$Ta_{1-x}N$, the amorphous boron remains dispersed in the material until the mechanical energy is high enough to trigger the formation of o-TaB. However, when the molar ratio of boron is higher than tantalum, a mixture of phases is obtained.

5 Acknowledgements

T. Garcia-Mendoza acknowledges the scholarship granted by CONACyT. E. A. Juarez-Arellano thanks Goethe-Universität for financial support during

his sabbatical leave. The authors also acknowledge the funding provided by CONACyT (LN-2015-01-260860, INFRA-2015-01-252013, LN-2016-271911, and FC-2015-2-947).

Table 1
Lattice parameters of δ-TaN from Le Bail fits of samples ball-milled 30 min (Figure 1). To evaluate the reproducibility several repetitions (R#) were done. The δ-TaN has B1 structure, space group $Fm\bar{3}m$.

System	Phase	a / Å	V_0 / Å^3	Repetition
Ta-BN-1:1	δ-TaN	4.367(3)	83.3(1)	R0
		4.378(4)	83.9(1)	R1
		4.376(8)	83.8(4)	R2
		4.365(3)	83.2(1)	R3
		4.364(3)	83.1(1)	R4
Ta-BN-2:1	δ-TaN	4.360(4)	82.9(1)	R0
		4.357(4)	82.7(1)	R1
		4.367(5)	83.3(2)	R2
		4.363(3)	83.1(1)	R3
		4.361(3)	83.0(1)	R4
ICSD	δ-TaN	4.317	80.4	(Shen and Wang 2011)
		4.32	80.6	(Lee et al. 2013)
		4.356	82.6	(Liu et al. 2012)
		4.33-4.42	81.2-86.4	(Matenoglou et al. 2008)
		4.383	84.2	(Elangovan et al. 2011)

Table 2
Lattice parameters and crystal structure from the Rietveld refinement of the X-ray powder diffraction patterns of Ta-BN (1:1) after 40 min of high-energy ball-milling (see Figure 2).

	δ-TaN	TaB	WC
Lattice Parameters			
a / Å	4.3863(3)	3.262(1)	2.9067(4)
b / Å	-	8.690(2)	-
c / Å	-	3.157(1)	2.838(4)
V / Å^3	84.39(1)	89.49(4)	20.77(1)
Structure			
Space Group	$Fm\bar{3}m$	$Cmcm$	$P\bar{6}m2$
Atoms	Ta; N	Ta; B	W; C
Wyckoff position	4a; 4b	4c; 4c	1a; 1f
Positions	0,0,0; $\frac{1}{2},\frac{1}{2},\frac{1}{2}$	0,0.141(1),$\frac{1}{4}$; 0,0.584(5),$\frac{1}{4}$	0,0,0; $\frac{2}{3},\frac{1}{3},\frac{1}{2}$
Occupation	0.84(1); 1.0	1.0; 1.0	1.0; 1.0
B (Å^2)	3.99(3)	2.75(9)	5.26(2)
Fract. / %	83.0(6)	7.9(2)	9.1(2)
Reliability factors			
χ^2	5.7	R_{wp}	6.38
R_p	4.53	R_{exp}	1.95
Data points	6412	Independent parameters	22

Table 3
Lattice parameters of products from the reaction of Ta-B, Ta-C and Ta-B-C of samples ball-milled up to 30 min (Figures 4).

System	Phase	a, b, c / Å	V / Å^3	S. G.
Ta - B				
Ta-B-1:1	TaB	3.244(1), 8.666(5), 3.136(2)	88.18(8)	$Cmcm$
	WC	2.898(1), 2.833(1)	20.82(1)	$P\bar{6}m2$
Ta-B-2:1	TaB_2	3.092(1), 3.235(2)	26.78(2)	$P6/mmm$
	TaB	3.287(2), 8.381(4), 3.190(1)	87.89(7)	Cmcm
	WC	2.909(1), 2.856(1)	20.93(1)	$P\bar{6}m2$
Ta - C				
Ta-C-1:1	TaC	4.428(3)	86.8(1)	$Fm\bar{3}m$
	WC	2.896(3), 2.850(4)	20.71(4)	$P\bar{6}m2$
Ta-C-2:1	TaC	4.374(3)	83.7(1)	$Fm\bar{3}m$
	WC	2.902(3), 2.840(2)	20.71(3)	$P\bar{6}m2$
Ta - B - C				
Ta-B-C-1:1:1	TaC	4.445(2)	87.81(8)	$Fm\bar{3}m$
	WC	2.885(3), 2.850(3)	20.53(3)	$P\bar{6}m2$
Ta-B-C-1:2:1	TaB_2	3.089(2), 3.238(4)	26.76(4)	$P6/mmm$
	TaC	4.456(3)	88.5(1)	$Fm\bar{3}m$
	WC	2.906(2), 2.843(3)	20.79(4)	$P\bar{6}m2$
Lattice Parameter from the database ICSD				
ICSD	TaB	3.28, 8.67, 3.15	89.72	ICSD-602892
	TaB_2	3.083, 3.24	26.7	ICSD-615525
	TaC	4.453	88.30	ICSD-159875
	WC	2.90, 2.85	20.79(4)	ICSD-246149

Table 4
Lattice parameters of products from the repetitions on the mechanosynthesis of Ta-B-C (1:1:1 and 1:2:1) ball-milled 30 min (Figures 4).

System	Phase	a, b, c / Å	V / Å^3	Repetition
Ta-B-C-1:1:1	TaC	4.446(4)	87.9(1)	R1
	TaC	4.442(4)	87.6(1)	R2
	TaC	4.446(3)	87.87(8)	R3
	TaC	4.444(3)	87.75(9)	R4
Ta-B-C-1:2:1	TaB_2	3.089(5), 3.241(4)	26.78(5)	R1
	TaC	4.454(3)	88.4(4)	
	TaB_2	3.093(3), 3.245(4)	26.88(4)	R2
	TaC	4.458(3)	88.6(1)	
	TaB_2	3.091(2), 3.242(3)	26.82(4)	R3
	TaC	4.459(3)	88.7(1)	
	TaB_2	3.091(2), 3.238(3)	26.79(3)	R4
	TaC	4.462(3)	88.8(1)	

References

A. Friedrich, B. Winkler, E. A. Juarez-Arellano, L. Bayarjarga, Review: Synthesis of binary transition metal nitrides, carbides and borides from the elements in the laser-heated diamond anvil cell and their structure-property relations, Materials 4 (10) (2011) 1648–1692.

H. O. Pierson, Handbook of refractory carbides, Noyes Publication, 1996.

S. T. Oyama, The Chemistry of Transition Metal Carbides and Nitrides, Springer Netherlands, Dordrecht, 1996, Ch. Introduction to the chemistry of transition metal carbides and nitrides, pp. 1–27.

Y. Tian, B. Xu, Z. Zhao, Microscopic theory of hardness and design of novel superhard crystals, International Journal of Refractory Metals and Hard

Materials 33 (2012) 93–106.

C. A. Escobar, J. C. Caicedo, W. Aperador, Corrosion resistant surface for vanadium nitride and hafnium nitride layers as function of grain size, Journal of Physics and Chemistry of Solids 75 (2014) 23–30.

W. G. Fahrenholtz, G. E. Hilmas, Ultra-high temperature ceramics: Materials for extreme environments, Scripta Materialia 129 (2017) 94–99.

Z. Wang, J. Wang, J. Hou, K. Huang, S. Jiao, H. Zhu, Facile synthesis of efficient photocatalytic tantalum nitride nanoparticles, Materials Research Bulletin 47 (2012) 3605–3611.

M. Takeyama, Properties of TaNx films as diffusion barriers in the thermally stable Cu/Si contact systems, Journal of Vacuum Science & Technology B 14 (2) (1996) 674.

T. Laurila, K. Zeng, J. Kivilahti, J. Molarius, T. Riekkinen, I. Suni, Tantalum carbide and nitride diffusion barriers for Cu metallisation, Microelectronic Engineering 60 (2002) 71–80.

Y. M. Lu, R. J. Weng, W. S. Hwang, Y. S. Yang, Study of phase transition and electrical resistivity of tantalum nitride films prepared by DC magnetron sputtering with OES detection system, Thin Solid Films 398-399 (2001) 356–360.

D. W. Lee, Y. N. Kim, M. Y. Cho, P. J. Ko, D. Lee, S. M. Koo, K. S. Moon, J. M. Oh, Reliability and characteristics of magnetron sputter deposited tantalum nitride for thin film resistors, Thin Solid Films 660 (2018) 688–694.

M. Lemberger, S. Thiemann, A. Baunemann, H. Parala, R. A. Fischer, J. Hinz, A. J. Bauer, H. Ryssel, MOCVD of tantalum nitride thin films from TBTEMT single source precursor as metal electrodes in CMOS applications, Surface and Coatings Technology 201 (2007) 9154–9158.

L. Gladczuk, A. Patel, C. S. Paur, M. Sosnowski, Tantalum films for protective coatings of steel,, Thin Solid Films 467 (2004) 150–157.

N. D. Cuong, D. J. Kim, B. D. Kang, S. G. Yoon, Structural and electrical characterization of tantalum nitride thin film resistors deposited on AlN substrates for π-type attenuator applications, Materials Science and Engineering: B 135 (2006) 162–165.

Y. X. Leng, H. Sun, P. Yang, J. Y. Chen, J. Wang, G. J. Wan, N. Huang, X. B. Tian, L. P. Wang, P. K. Chu, Biomedical properties of tantalum nitride films synthesized by reactive magnetron sputtering, Thin Solid Films 398–399 (2001) 471–475.

W. Jin, G. Wang, X. Peng, W. Li, A. M. Qasim, P. K. Chu, Tantalum nitride films for corrosion protection of biomedical Mg-Y-RE alloy, Journal of Alloys and Compounds 764 (2018) 947–958.

J. Gatterer, G. Dufek, P. Ettmayer, H. Kieffer, Das kubisehe Tantalmononitrid (B 1-Typ) und seine Mischbar - keit mit den isotypen Ubergangsmetallnitriden und -carbiden, Monatshefte für Chemie 106 (1975) 1137–1147.

K. Frisk, Analysis of the phase diagram and thermochemistry in the Ta-N and the Ta-C-N systems, Journal of Alloys and Compounds 278 (1998) 216–226.

A. Friedrich, B. Winkler, L. Bayarjargal, E. A. Juarez-Arellano, W. Morgenroth, J. Biehler, F. Schröder, J. Yan, S. M. Clark, In situ observation of the reaction of tantalum with nitrogen in a laser heated diamond anvil cell, Journal of Alloys and Compounds 502 (2010) 5–12.

A. Friedrich, W. Morgenroth, L. Bayarjargal, E. A. Juarez-Arellano, B. Winkler, B. Konôpková, In situ study of the high-pressure high-temperature stability field of TaN and of the compressibilities of ϑ-TaN and TaON, High Pressure Research 33 (3) (2013) 633–641.

A. Salamat, K. Woodhead, S. I. U. Shah, A. L. Hector, P. F. McMillan,

Synthesis of $U_3Se_5$and U_3Te_5type polymorphs ofTa_3N_5 by combining high pressure-temperaturepathways with a chemical precursor approach, Chemical Communications 50 (2014) 10041–10044.

C. L. Yeh, E. W. Liu, Y. C. Chang, Effect of preheating on synthesis of tantalum nitride by self-propagating combustion, Journal of the European Ceramic Society 24 (2004) 3807–3815.

C. Angelkort, A. Berendes, H. Lewalter, W. Bock, B. Kolbesen, Formation of tantalum nitride films by rapid thermal processing, Thin Solid Films 437 (2003) 108–115.

L. Shen, N. Wang, Effect of Nitrogen Pressure on the Structure of Cr-N, Ta-N, Mo-N, and W-N Nanocrystals Synthesized by Arc Discharge, Journal of Nanomaterials 2011 (2011) 1–5.

Y. J. Lee, D. Y. Kim, H. H. Nersisyan, K. H. Lee, M. H. Han, K. S. Kang, K. K. Bae, J. H. Lee, Rapid solid-phase synthesis for tantalum nitride nanoparticles and coatings, International Journal of Refractory Metals and Hard Materials 41 (2013) 162–168.

L. Liu, K. Huang, J. Hou, H. Zhu, Structure refinement for tantalum nitrides nanocrystals with various morphologies, Materials Research Bulletin 47 (2012) 1630–1635.

P. P. George, A. Gedanken, S. B. D. Makhlouf, I. Genish, A. Marciano, R. Abu-Mukh, Synthesis and characterization of titanium nitride, niobium nitride, and tantalum nitride nanocrystals via the RAPET (reaction under autogenic pressure at elevated temperature) technique, Journal of Nanoparticle Research 11 (2009) 995–1003.

Y. Qin, L. Liu, L. Chen, Characterization of nanocrystalline tantalum nitride formed by solid-gas reaction during mechanical alloying, Journal of Alloys and Compounds 269 (1998) 238–240.

Y. H. Yang, D. J. Chen, F. B. Wu, Microstructure, hardness, and wear resistance of sputtering TaN coating by controlling RF input power, Surface & Coatings Technology 303 (2016) 32–40.

L. G. Boiko, S. V. Popova, Crystal structure and superconducting properties of tantalum nitride obtained at high pressures, Journal of Experimental and Theoretical Physics Letters (USSR) 12 (1970) 70–71.

T. Mashimo, S. Tashiro, T. Toya, M. Nishida, H. Yamazaki, S. Yamaya, K. Oh-Ishi, S. Syono, Synthesis of the B1-type tantalum nitride by shock compression, Journal of Materials Science 28 (1993) 3439–3443.

E. Gillan, R. B. Kaner, Rapid solid-state synthesis of refractory nitrides, Inorganic Chemistry 33 (1994) 5693–5700.

C. H. Ma, W. F. Zhang, J. L. He, H. M. Zhu, Synthesis and characterization of tantalum nitride nanopowder prepared through homogeneous reaction, Transactions of Nonferrous Metals Society of China 17 (S1) (2007) s556–s559.

W. Ensinger, M. Kiuchi, M. Satou, Low-temperature formation of metastable cubic tantalum nitride by metal condensation under ion irradiation, Journal of Applied Physics 77 (1995) 6630–6635.

N. Koutná, D. Holec, O. Svoboda, F. F. Klimashin, P. H. Mayrhofer, Point defects stabilise cubic Mo-N and Ta-N, Journal of Physics D: Applied Physics 49 (2016) 375303.

F. Pacher, P. H. Mayrhofer, D. Holec, Vacancy-driven extended stability of cubic metastable Ta-Al-N and Nb-Al-N phases, Surface and Coatings Technology 326 (2017) 37–44.

T. Glechner, P. H. Mayrhofer, D. Holec, S. Fritze, E. Lewin, V. Paneta, D. Primetzhofer, S. Kolozsvári, H. Riedl, Tuning structure and mechanical properties of Ta-C coatings by N-alloying and vacancy population, Scientific

Reports 8 (2018) 17669.

M. G. Granados-Fitch, E. A. Juarez-Arellano, J. M. Quintana-Melgoza, M. Avalos-Borja, Mechanosynthesis of rhenium carbide at ambient pressure and temperature, International Journal of Refractory Metals and Hard Materials 55 (1) (2016) 11–15.

M. Kakazey, M. Vlasova, E. A. Juarez-Arellano, T. Torchynskac, V. A. Basiukd, Defect states and morphological evolution in mechanically processed ZnO + xC nanosystems as studied by EPR and photoluminescence spectroscopy, RSC Advances 6 (2016) 58709.

A. Martinez-Garcia, A. K. Navarro-Mtz, C. Neun, L. Bayarjargal, W. Mongenroth, E. Lopez-Vazquez, M. Avalos-Borja, B. Winkler, E. A. Juarez-Arellano, Effect of ball to powder ratio on the mechanosynthesis of Re_2C and its compressibility, Journal of Alloys and Compounds 10 (2) (2019) 34–40.

J. Rodriguez-Carvajal, Recent advances in magnetic structure determination by neutron powder diffraction, Physica B 192 (1993) 55–69.

A. R. Oganov, A. O. Lyakhov, Q. Zhu, 3.04 - theory of superhard materials, Reference Module in Materials Science and Materials Engineering, Comprehensive Hard Materials 3 (2014) 59–79.

L. Zhai, Z. Liu, C. Li, X. Qu, Q. Zhang, G. Li, X. Zhanga, B. Abdel-Magid, Cyanate ester resin based composites with high toughness and thermal conductivity, RSC Advences 9 (2019) 5722–5730.

E. Aradi, S. R. Naidoo, D. G. Billing, D. Wamwangi, I. Motochi, T. E. Derry, Ion beam modification of the structure and properties of hexagonal boron nitride: an infrared and X-ray diffraction study, Nuclear Instruments and Methods in Physics Research B 331 (2014) 140–143.

A. K. Niessen, F. R. Boer, The enthalpy of formation of solid borides, carbides,

nitrides, silicides and phosphides of transition and noble metals, Journal of the Less-Common Metals 82 (1981) 75–80.

S. V. Meschel, O. J. Kleppa, Thermochemistry of alloys of transition metals and lanthanide metals with some IIIB and IVB elements in the periodic table, Journal of Alloys and Compounds 321 (2001) 183–200.

D. Li, F. Tian, D. Duan, K. Bao, B. Chu, X. Sha, B. Liu, T. Cui, Mechanical and metallic properties of tantalum nitrides from first-principles calculations, RSC Advances 4 (2014) 10133–10139.

X. OuYang, F. Yin, J. Hu, Y. Liu, Z. Lon, Thermodynamic Modeling of B-Ta and B-C-Ta Systems, Journal of Phase Equilibria and Diffusion 38 (2017) 874–886.

B. Winkler, E. A. Juarez-Arellano, A. Friedrich, L. Bayarjargal, F. Schröder, J. Biehler, V. Milman, S. M. Clark, J. Yan, In situ synchrotron X-ray diffraction study of the formation of TaB_2 from the elements in a laser heated diamond anvil cell, Solid State Sciences 12 (2010) 2059–2064.

S. T. Lin, C. Lee, Growth of tantalum boron nitride films on Si by radio frequency reactive sputtering: effect of N_2/Ar flow ratio, Materials Chemistry and Physics 82 (2003) 691–697.

A. A. Goncharov, V. V. Petukhov, S. N. Dub, V. A. Konovalov, Structure, electrophysical, and mechanical properties of Ta-B-N films, The physics of metals and metallography 105 (2008) 362–367.

M. P. Savyak, O. B. Melnick, M. A. Vasil'kivska, I. I. Timofeeva, V. I. Ivchenko, I. V. Uvarova, Mechanical Synthesis of Tantalum Borides and Modeling of Solid Solutions of Boron in Tantalum, Powder Metallurgy and Metal Ceramics 57 (7-8) (2018) 373–383.

L. Bayarjargal, B. Winkler, A. Friedrich, E. A. Juarez-Arellano, Synthesis of TaC and Ta_2C from tantalum and graphite in the laser-heated diamond

anvil cell, Chinese Science Bulletin 59 (2014) 5283.

A. I. Gusev, A. S. Kurlov, V. N. Lipatnikov, Atomic and vacancy ordering in carbide ζ-Ta_4C_{3-x} ($0.28 \leq x \leq 0.40$) and phase equilibria in the Ta-C system, Journal of Solid State Chemistry 180 (2007) 3234–3246.

M. Thommes, K. Kaneko, A. V. Neimark, J. P. Oliver, F. Rodriguez-Reinoso, J. Rouquerol, K. S. W. Sing, Physisorption of gases, with special reference to the evaluation of surface area and pore size distribution (IUPAC Technical Report), Pure and Applied Chemistry 87 (2015) 1051–1069.

S. J. Gregg, K. S. W. Sing, Adsorption, surface area and porosity, 2nd Edition, Academic Press, 1982.

K. S. W. Sing, R. T. Williams, Physisorption hysteresis and the characterization of nanoporous materials, Adsorption Science & Technology 22 (2004) 773–782.

J. C. Groen, A. A. Louk, J. Perez-Ramirez, Pore size determination in modified midro- and mesoporous materials. Pitfalls and limitations in gas adsorption data analysis, Microporous and Mesoporous Materials 60 (2003) 1–17.

P. B. Mirkarimi, K. F. McCarty, D. L. Medlin, Review of advances in cubic boron nitride film synthesis, Materials Science and Engineering: R: Reports 21 (1997) 47–100.

A. Mujica, A. Rubio, A. Muñoz, R. J. Needs, High-pressure phases of group-IV, III–V, and II–VI compounds, Reviews of Modern Physics 75 (2003) 863–912.

G. M. Matenoglou, L. E. Koutsokeras, C. E. Lekka, G. Abadias, S. Camelio, G. A. Evangelakis, C. Kosmidis, P. Patsalas, Optical properties, structural parameters, and bonding of highly textured rocksalt tantalum nitride films, Journal of Applied Physics 104 (2008) 124907.

T. Elangovan, S. Murugeshan, D. Mangalaraj, P. Kuppusami, S. Khan,

C. Sudha, V. Ganesan, R. Divakar, E. Mohandas, Synthesis and high temperature XRD studies of tantalum nitride thin films prepared by reactive pulsed dc magnetron sputtering, Journal of Alloys and Compounds 509 (2011) 6400–6407.